Responses of phytoplankton communities to internal waves in oligotrophic oceans

Lingqi Ma,[1,2,3] Xiaolin Bai,[2] Edward A Laws,[4] Wupeng Xiao,[1]*
Cui Guo,[5] Xin Liu,[1] Kuo-Ping Chiang,[3] Kunshan Gao,[2] Bangqin Huang[1]*

[1]State Key Laboratory of Marine Environmental Science / Fujian Provincial Key Laboratory for Coastal Ecology and Environmental Studies / College of the Environment and Ecology, Xiamen University, Xiamen, Fujian.
[2]State Key Laboratory of Marine Environmental Science / College of the Ocean and Earth Sciences, Xiamen University, Xiamen, Fujian.
[3]Institute of Marine Environmental Chemistry and Ecology, National Taiwan Ocean University, 202-24 Keelung, Taiwan.
[4]Department of Environmental Sciences, College of the Coast & Environment, Louisiana State University, Baton Rouge, Louisiana 70803, USA.
[5]College of Marine Life Science, Ocean University of China, Qingdao, Shandong.

***Corresponding authors**:
Dr. Wupeng Xiao, tel: 86-18959207758, email: wpxiao@xmu.edu.cn
Dr. Bangqin Huang, tel: 86-592-2187783, email: bqhuang@xmu.edu.cn

Key Points:

- We provided strong evidence that there is internal wave activity at the oligotrophic basin of the South China Sea
- The temporal variations of phytoplankton communities in the upper, middle, and lower layers of the euphotic zone differ
- The perturbation caused by internal waves made the three-layer structure of the phytoplankton community in oligotrophic oceans apparent

Abstract

Nutrients associated with internal waves are known to perturb phytoplankton communities in oligotrophic oceans, but details of the relevant processes and mechanisms are unclear. Here we report insights about the impacts of internal waves on the phytoplankton community based on 154-hour time-series of observations in an oligotrophic basin of the South China Sea. We found that the temporal variations of phytoplankton communities in the upper, middle, and lower layers of the euphotic zone differ. We demonstrated that these changes probably resulted from the perturbation caused by internal waves. These results suggest that the structure of the phytoplankton community in oligotrophic oceans is best described by a three-layer system at steady state and that the perturbation caused by internal waves helps to reveal this structure. We believe that the paradigm of this three-layer structure will provide a new theoretical framework for the study of phytoplankton-based biogeochemical processes in oligotrophic oceans.

Plain Language Summary

Internal waves are a widespread phenomenon in stratified oceans. They are especially important in oligotrophic oceans because they can provide the dominant source of nutrient supply to the euphotic zone. This process is expected to enhance the phytoplankton biomass and primary productivity and change the phytoplankton community, but details of the relevant processes and mechanisms are still unclear. Based on results from satellite image, 154 hours of time series observations, and model output, we provided strong evidence that there is internal wave activity at the SEATS station in the South China Sea. The patterns of change of the phytoplankton community in the upper, middle, and lower layers of the euphotic zone differed during our observations. We demonstrated that these changes were resulted from the perturbation caused by internal waves. We therefore hypothesized that the structure of the phytoplankton community in the euphotic zone of oligotrophic oceans is best described by a three-layer structure at steady state. The perturbation caused by internal waves made this structure apparent because the factors that limited phytoplankton growth differed in the three layers. This novel concept will facilitate estimates of marine primary production and enhance understanding of the global carbon cycle.

Introduction

Internal waves are widely present in stratified oceans and play an important role in promoting the movement of water masses and the exchange of nutrients and materials (Garwood et al., 2020; Whalen et al., 2020). In oligotrophic oceans, mixing driven by internal waves can dominate the supply of nutrients to the euphotic zone (Tuerena et al., 2019), which in turn stimulates phytoplankton primary productivity (Lucas et al., 2011). Studies of how the phytoplankton community responds to internal waves have concentrated mainly on upwelling regions, where nutrients are relatively abundant (Ma et al., 2020; Omand et al., 2011; Villamaña et al., 2017). There have been few similar studies in oligotrophic oceans.

The euphotic zone of oligotrophic oceans can be divided into a nutrient-depleted layer (NDL) above the nutricline and a light-limited layer or nutrient-replete layer (NRL) below the NDL (Du et al., 2017; Dugdale, 1967). However, the transition region between limitation by light or nutrients in oligotrophic oceans is usually characterized by a deep chlorophyll maximum layer (DCML), where light and nutrients are co-limiting and the rates of growth and loss of phytoplankton are usually in dynamic equilibrium (Chen et al., 2013; Guo et al., 2014; Landry et al., 2011b). In the euphotic zone below the DCML, grazing exceeds phytoplankton growth (Landry et al., 2011a). These scenarios suggest that the phytoplankton community in the euphotic zone of oligotrophic oceans may be characterized by a three-layer structure under steady state conditions: the upper portion of the NDL, where phytoplankton growth is strictly limited by nutrients; a middle layer, the DCML, where light and nutrients are co-limiting and phytoplankton gains and losses are in a dynamic equilibrium; and a light-limited region below the DCML, the NRL, where nutrients are abundant and the grazing pressure is the greatest. We hypothesized that if this

system were perturbed by an influx of allochthonous nutrients from the bottom of the euphotic zone by internal waves, the differences of the physiological conditions of the phytoplankton in each layer would cause their responses to differ in ways that would clearly reveal the three-layer structure.

To test this hypothesis, we used 154 hours of data collected from the SouthEast Asia Time-series Study (SEATS, 116°E, 18°N) station during a cruise in the northern South China Sea (SCS) during the summer of 2014. The northern SCS basin is a typical oligotrophic ocean, and the SEATS station, located in the center of the northern SCS basin, is a site often used to study the biogeochemical characteristics of oligotrophic oceans (Wong et al., 2007). The Luzon Strait, which borders the SCS on the east, generates energetic internal waves that radiate both eastward and westward. The energy of these internal waves is concentrated mainly in internal tides (Lin et al., 2020), i.e., internal waves of tidal frequency. In the SCS, the energy fluxes of semidiurnal internal tides propagate mainly toward the northwest (Zhao, 2014; 2020). These onshore, radiating, semidiurnal internal tides finally evolve into nonlinear internal solitary waves and dissipate on the continental shelf. In contrast, diurnal internal tides radiate toward the southwest and mainly affect the center of the SCS (Zhao, 2020), as shown in Figure 1a. The northern SCS basin is therefore an area into which diurnal, internal waves from the Luzon Strait radiate and is an ideal region to test our hypothesis.

Data and Methods

Sampling and Measurements

Field observations were conducted onboard the R/V *Shiyan 1* and lasted from 10:30 on 23 August to 20:30 on 29 August at the SEATS station (Figure 1a). Water

temperature, salinity, and pressure were recorded during each cast with a SeaBird model SBE9/11 conductivity-temperature-depth (CTD) recorder. A total of 40 CTD casts were conducted at different time intervals, including at least every 6 hours from 02:00 on 25 August to 22:00 on 27 August. Seawater samples for nutrient analyses were collected from depths of 5, 25, 50, 75, and 100 m on the first cast. The concentrations of nitrate plus nitrite (NOx, μmol L^{-1}) were measured with a QUAATRO nutrient analyzer.

Seawater samples for phytoplankton pigment analyses were collected from the same depths sampled for nutrient concentrations every 6 hours from 02:00 on 25 August to 22:00 on 27 August. Thirteen marker pigments were quantified by high performance liquid chromatography (HPLC) following the modified method of Furuya et al. (2003). We then used the CHEMTAX program (Mackey et al., 1996) to calculate the relative contributions of 9 phytoplankton groups to the total Chlorophyll *a* (TChl *a*, the sum of Chl *a* and Divinyl Chl *a*). These procedures have previously been reported in detail (Ma et al., 2020; Xiao et al., 2018) and are described briefly in Text S1.

Field incubation experiments

To determine the nitrate assimilation rate (ρNO_3^-), new production (NP), and gross primary production (GPP), water samples were collected in acid-cleaned bottles from depths of 3, 17, 33, 55, and 110 m, corresponding to light intensities of about 66%, 50%, 25%, 10%, and 1% of the surface irradiance, respectively. ρNO_3^- was measured daily following the method of Dugdale and Wilkerson (1986). Incubation procedures and subsequent calculations of the ρNO_3^- have previously been reported in detail (Ma et al., 2020) and are described in Text S2.

Seawater samples of 10 L were collected from depths of 5 m, 25 m, 50 m, 75 m,

and 110 m during the second day (24 August) to conduct dilution experiments for the measurement of phytoplankton growth rates (μ) and microzooplankton grazing rates (m) (Landry and Hassett, 1982; Landry et al., 2008) (Text S3).

Simulation of internal tides

The characteristics and influence of internal waves at the SEATS station were analyzed using the 26-year-coherent satellite altimeter results of Zhao (2020) (Figure 1a) based on a new mapping technique that combines plane wave analysis with 2-D band-pass filtering. The output from the MITgcm LLC4320, a state-of-the-art submesoscale-permitting global ocean circulation model, was also used to analyze the characteristics of internal wave at the SEATS station. The genesis and propagation of internal waves could therefore be seen from the altimeter results, while their structures in the ocean interior were revealed by the LLC4320.

The LLC4320 provides one of the most high-resolution and advanced hydrodynamic outputs at present, with a horizontal grid spacing of $1/48^{o}$ and 90 vertical levels (Forget et al., 2015; Torres et al., 2018). The model outputs included sea level height, potential temperature, salinity, and velocity, for a period of 14 months from 13 September 2011 to 15 November 2012 at intervals of 1 h. The LLC output is available from the ECCO project (https://data.nas.nasa.gov/ecco/data.php). Because there were no simulation results during our observation period, we first determined the relationship between internal waves and barotropic tides from the model output at the SEATS station, and then we used that relationship and barotropic tide data to predict the characteristics of internal waves at SEATS during our observations. Tidal information was obtained from the regional tidal solution of the OSU TPXO Tide Models using Tide Model Driver (TMD) Matlab Toolbox (https://www.esr.org/research/polar-tide-models/tmd-software/).

Results

Internal tides from observations and numerical simulations

The influence of internal waves at the SEATS station was revealed by satellite and field observations (Figure 1), as well as results of the simulations. The 26-year-coherent satellite altimeter results indicated that internal waves at SEATS were mainly diurnal internal tides. After their generation in the Luzon Strait, the diurnal, internal tides propagated southwestward, as shown by the energy fluxes and phases of the internal tides in Figure 1a. It took about 1.5–2 days for these waves to reach SEATS from the Luzon Strait.

As expected, direct evidence of the presence of internal waves during our field observations was provided by a MODIS true color image obtained at 05:25 on 28 August 2014 (Figure 1b). In this image, which has a spatial resolution of 250 m, surface imprints of internal waves are apparent near the Dongsha Atoll (117^{o}E, 20.6^{o}N). The signature was clear because of the nonlinear steepening of the internal wave during shoaling. The spatial distribution of the fronts of these internal waves was consistent with the phase of the K_1 internal tide (Figure 1b). The implication is that internal waves were present and influencing our field measurements. Moreover, field hydrographic observations revealed synchronous, diurnal fluctuations in the time-series of temperature, salinity, and density profiles as well as the depth of maximum buoyancy frequency (N^2) (Figure 1c). This synchrony provided further support that diurnal internal tides impacted conditions at the SEATS station during our observation period.

To overcome the limitation of the sampling frequency in our observations, we used the LLC4320 simulation results to show the characteristics of internal waves at the SEATS station (Figure S1). Consistent with our observation and analysis, the

simulation results showed periodic fluctuations of isopycnals in the upper 300 m throughout August 2012 (Figure S1c), an indication of diurnal internal tides. The barotropic tides in the Luzon Strait and at SEATS were basically in phase during August 2012 (Figure S1a,b), but the largest-amplitude internal waves at SEATS lagged the spring tide in the Luzon Strait by 2–3 days (Figure S1). This time lag is consistent with the propagation time of internal waves from the Luzon Strait to SEATS (Figure 1a). We could therefore use the barotropic tidal phase to predict the internal tides at SEATS. Because the barotropic tides were similar in August 2014 and August 2012 and because our observations covered the period from the spring tide before 25 August to the neap tide on 27 August (Figure S2), the amplitude of the spring tide during our observations was presumably as much as ~30 m (Figure S1c). This conclusion is consistent with our hydrographic observations (Figure 1c).

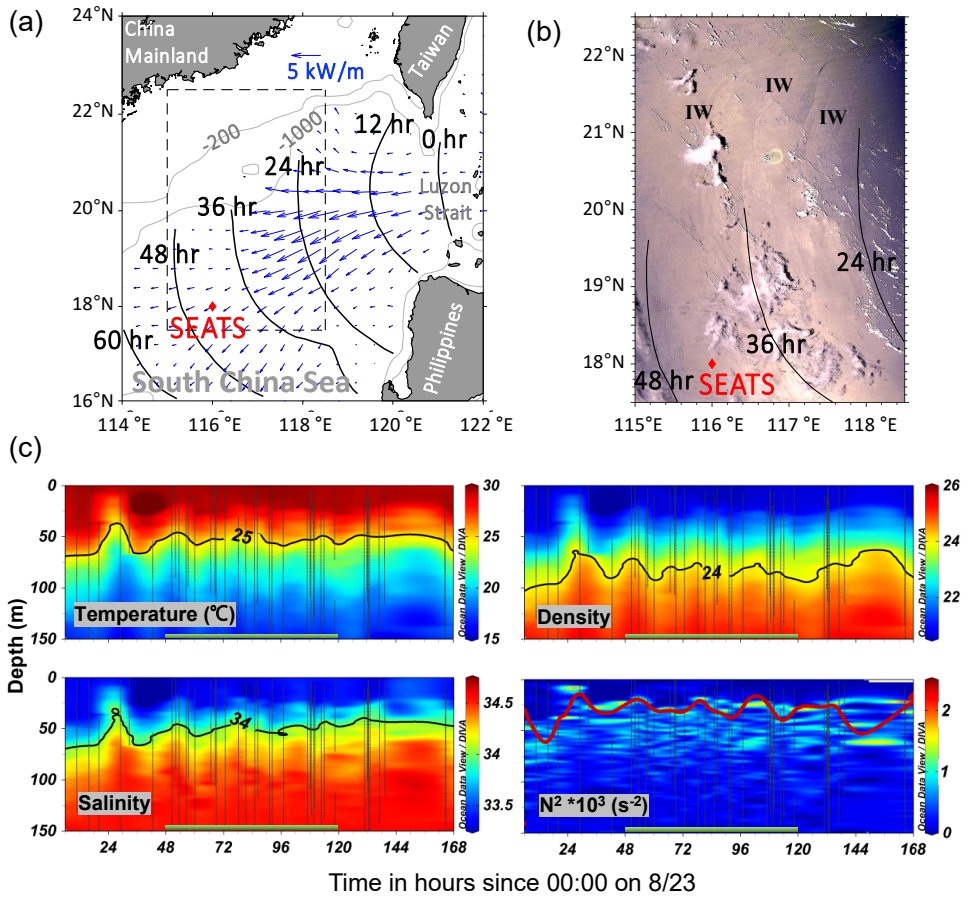

201

202 **Figure 1.** Field-sampling station in the South China Sea basin in summer 2014 and its
203 hydrographic characteristics. (a) Location of the SEATS station (red diamond). Blue
204 arrows show depth-integrated energy fluxes and black contours show propagating
205 time of the K_1 internal tide from the Luzon Strait, based on the results of Zhao (2020).
206 (b) MODIS true color image taken at 05:25 on 28 August 2014, with the propagating
207 time of K_1 internal tide from the Luzon Strait. (c) Temporal variations of
208 hydrographic parameters at SEATS, where N^2 is the squared buoyancy frequency, and
209 the red solid line indicates the depth of maximum N^2.

210

Vertical and temporal distributions of phytoplankton biomass and community composition

The TChl *a* concentration initially increased and then decreased with depth, and the DCML appeared at 75 m (Figure S4). The dominant phytoplankton groups were mainly *Prochlorococcus* and *Synechococcus* above the DCML and *Prochlorococcus* and Haptophytes_8 below the DCML. During the three-day observation period, there were significant changes of the concentrations of TChl *a* and the relative abundances of the main phytoplankton groups. The patterns of change varied between depths (Figure 2). The concentration of TChl *a* in the upper 50 m increased significantly over time (Figure 2a), but there was no obvious temporal trend at 75 m and 100 m (Figure 2b, c). The changes of the phytoplankton community were attributable mainly to significant changes in the relative abundances of *Prochlorococcus* and *Synechococcus* during the observation period. The relative abundance of *Prochlorococcus* (quantified by the ratio of its marker pigment divinyl chlorophyll *a* to TChl *a*, i.e., Dv-Chl/TChl) increased significantly in the upper 50 m (Figure 2d) and decreased significantly at 100 m (Figure 2d, e), but there was no obvious change at 75 m (Figure 2f). The relative abundance of *Synechococcus* (represented by the ratio of its marker pigment zeaxanthin to TChl *a*, Zea/TChl) decreased significantly in the upper 50 m (Figure 2g), but there was no obvious trend at 75 m and 100 m (Figure 2h, i).

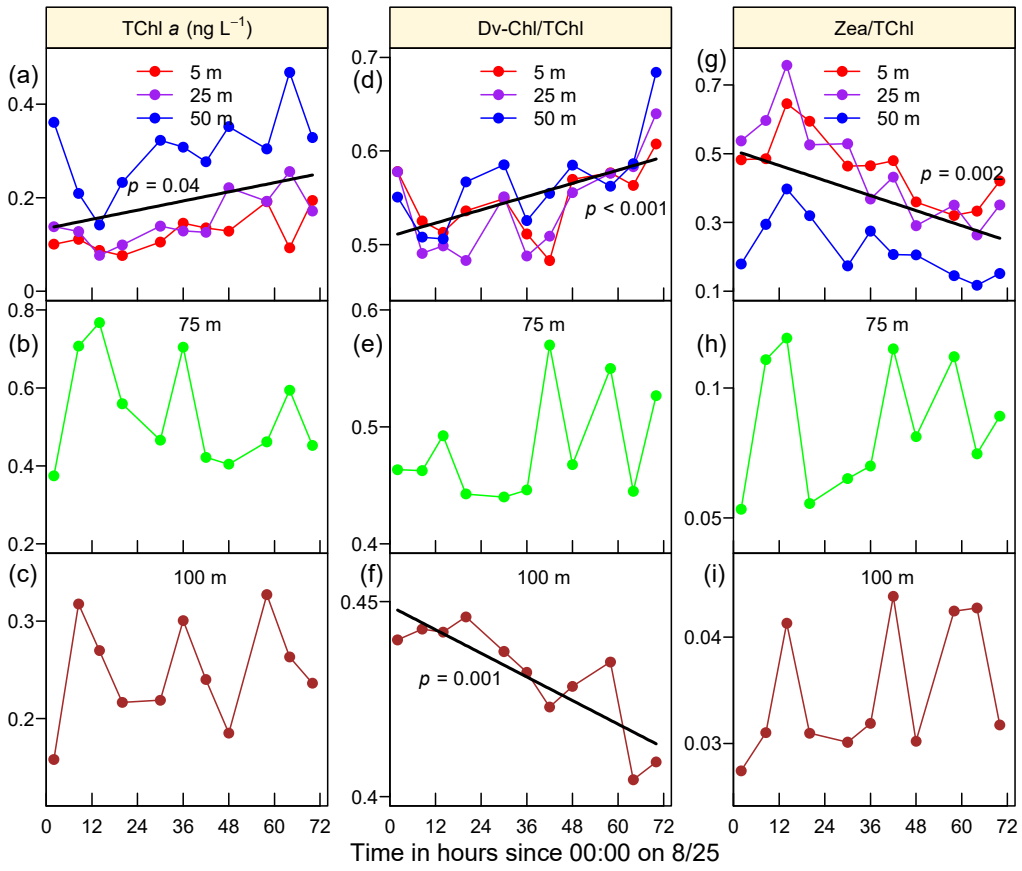

231

232 **Figure 2.** Temporal variations of phytoplankton biomass and community composition

233 in different layers at the SEATS station. (a–c) TChl *a*; (d–f) The relative abundance of

234 *Prochlorococcus* (represented by the ratio of its marker pigment divinyl chlorophyll *a*

235 to TChl *a*, Dv-Chl/TChl); (g–i) The relative abundance of *Synechococcus*

236 (represented by the ratio of its marker pigment zeaxanthin to TChl *a*, Zea/TChl).

237

238

Process rates and production

The ρNO_3^- underwent obvious changes during the 7-day observation period. High values at 55 m and 110 m were particularly noteworthy on the second day (24 August) and third day (25 August) (Figure 3a), which corresponded to the time when the uplift of the thermocline, halocline, and pycnocline occurred (Figure 1c). The value of ρNO_3^- was highest at 55 m, extremely low in the upper 33 m, and intermediate at 110 m (Figure 3b). The ρNO_3^- estimated with a generalized additive model (GAMs, Text S4) reached a maximum at a depth of about 75 m (Figure 3b). New production (NP) estimated from the ρNO_3^- was significantly lower than gross primary production (GPP) above 75 m, but the gap gradually narrowed at greater depths (Figure S5).

The phytoplankton growth rates and microzooplankton grazing rates agreed well with previous averages in the SCS (Figure 3c). In general, the growth rate exceeded the grazing rate above the DCML, the two rates were basically in balance at the DCML, and the growth rate was less than the grazing rate below the DCML. The grazing pressure (the ratio of grazing rate to growth rate, m/μ) increased from the surface to 110 m.

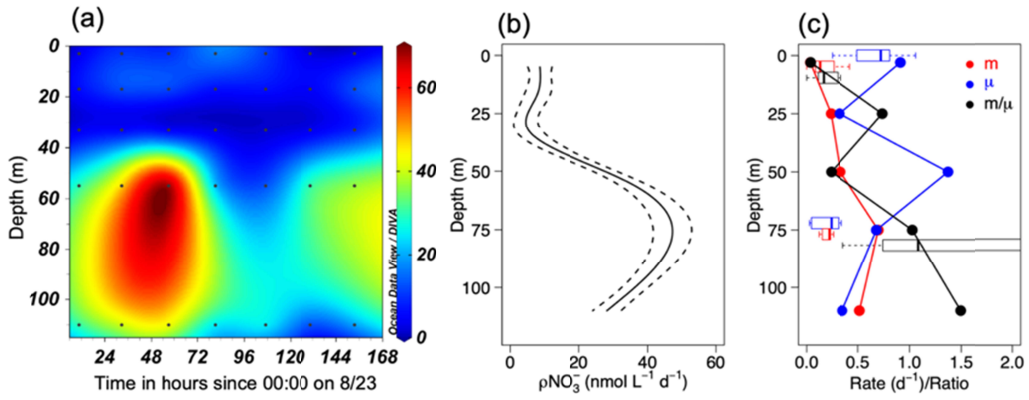

Figure 3. (a) Temporal variations of nitrate assimilation rate; (b) The vertical profile of nitrate assimilation rate was fitted by generalized additive models (GAMs); (c) Vertical profiles of phytoplankton growth rate, microzooplankton grazing rate, and grazing pressure, where solid dots and lines were results obtained in this study and boxes were results obtained from Chen et al. (2013).

Discussion

We found that the temporal trends of TChl *a* and the dominant phytoplankton groups differed above, within, and below the DCML during our observation period (Figure 2). The differences between these trends suggested that the phytoplankton communities in these three layers were regulated by different environmental mechanisms. The results therefore supported our hypothesis that the structure of the phytoplankton community in oligotrophic oceans differs in the NDL, DCML, and NRL. Under steady-state conditions, the boundary between the DCML and NRL is not apparent (Figure S4), and the two-layer structure described by Dugdale (1967) and Du et al. (2017) adequately describes the phytoplankton community. However, under unstable conditions or when the system is perturbed, the difference between the DCML and NRL becomes apparent (Figure 2) and a three-layer structure analogous to what has been described by Landry et al. (2011a) emerges. We then asked whether internal waves might be responsible for this perturbation at SEATS.

The impact of internal waves on phytoplankton is mainly the result of an increase in the supply of allochthonous nutrients (Garrett, 2003; Sharples et al., 2009). These nutrients would have been taken up by phytoplankton if there had been adequate light in the lower layers of the euphotic zone. The ρNO_3^- in the lower euphotic zone (50–110 m) was higher during 23–25 August than afterward (Figure 3a), and 23–25 August was when the spring tides occurred (Figure S2). The implication is that strong internal wave activity during the spring tides enhanced the influx of nutrients from the nutricline into the lower layers of the euphotic zone. There is usually a time lag between the uptake of nutrients and the increase of phytoplankton chlorophyll (Ma et al., 2020; Sharples et al., 2007; Wang et al., 2007). Changes of the phytoplankton community would therefore have become apparent

after the spring tides. If nitrate were added at the base of the euphotic zone, *Prochlorococcus* would lose its competitive advantage because most *Prochlorococcus* ecotypes lack the ability to take up nitrate (Bouman et al., 2006), and other phytoplankton species with the ability to take up nitrate would benefit. This line of reasoning could well explain the significant decrease in the relative abundance of *Prochlorococcus* at 100 m (Figure 2f). However, the grazing pressure of microzooplankton on phytoplankton was relatively high at 100 m (Figure 3c), consistent with previous observations (Landry et al., 2011a), and the growth of phytoplankton was severely light limited at that depth (Figure 3c). The result was that the grazing of microzooplankton constrained the accumulation of phytoplankton biomass, and hence there was no increase of TChl *a* (Figure 2c). In the DCML (75 m), the allochthonous nutrients supplied by internal waves led to high phytoplankton growth rates due to relatively favorable irradiances and nutrient concentrations, but the high rate of microzooplankton grazing balanced the high growth rates (Figure 3c). Therefore, although there were diurnal fluctuations of the TChl *a* and the relative abundances of dominant groups in the DCML, there was no obvious trend in the composition or biomass of the phytoplankton community in the DCML during the 3 days of observation (Figure 2b, e, h). The microzooplankton were likely consumed by mesozooplankton (Fonda Umani et al., 2005), which can move vertically (Hays, 2003), and their upward migrations might therefore have resulted in excretion of ammonium into the NDL (King et al., 1987; Webb and Johannes, 1967). We did not directly determine ammonium concentrations and ammonium uptake rates, but the reduction of the NP/GPP ratio in the upper layers (Figure S5) was an indication that recycled ammonium became relatively more important than nitrate as a source of inorganic nitrogen. The fact that most *Prochlorococcus* can use the ammonium

314 excreted by zooplankton better than other phytoplankton such as *Synechococcus*
315 (Berube et al., 2015; Moore et al., 2002) may explain why the growth of
316 *Prochlorococcus* exceeded that of other phytoplankton in the upper 50 m (Figure 2d).
317 The phytoplankton in the NDL were not light-limited, and because the grazing
318 pressure of microzooplankton was low (Figure 3c), grazing could not control the
319 accumulation of phytoplankton biomass. This line of reasoning could explain the
320 increasing trend of TChl *a* in the NDL (Figure 2a). In summary, the likely impact of
321 internal waves was basically consistent with the different responses that revealed the
322 three-layer structure of the phytoplankton community.

323 To further test the internal wave hypothesis, we assumed that all the nitrate taken
324 up by phytoplankton within the 3 days (25–27 August) was converted into
325 phytoplankton biomass. We then compared the theoretical accumulation of
326 phytoplankton biomass in terms of chlorophyll *a* with the observed maximum change
327 of chlorophyll within the 3 days to determine whether the biomass supported by
328 nitrate equaled the change of total biomass. The results showed that the theoretical
329 accumulation of chlorophyll *a* was significantly lower than the observed maximum
330 change of chlorophyll *a* in the upper 50 m. The opposite was true at 100 m, and at the
331 DCML the two values were basically the same (Figure S6). The implication is that
332 even if the phytoplankton biomass produced from nitrate uptake accumulated
333 monotonically during the 3 days, the estimated net accumulation was still
334 significantly lower than the observed changes of chlorophyll in the upper 50 m. The
335 implication is that nitrate was not the only nitrogen source in the upper 50 m and
336 underscores the importance of ammonium nitrogen in controlling the dynamics of the
337 phytoplankton community in the NDL. In contrast, the fact that the theoretical
338 accumulation of chlorophyll *a* was significantly higher than the observed maximum

change of chlorophyll *a* at 100 m implies that there was a large loss of phytoplankton biomass produced from nitrate uptake. This conclusion is consistent with the intense grazing pressure from microzooplankton in the NRL (Figure 3c). The agreement between the theoretical and observed changes of chlorophyll *a* concentrations in the DCML was consistent with the dynamic balance between phytoplankton growth and microzooplankton grazing in this layer (Figure 3c).

Other environmental changes that occurred during our observation period included an anticyclonic warm eddy (Figure S7) and rain that occurred for a short time on 26 and 27 August. The impact of the warm eddy was obviously untenable because there was little chance for a warm eddy to fuel phytoplankton growth in the upper waters of the SCS basin both vertically and horizontally (Huang et al., 2010; Wang et al., 2018). The rainy weather could have been associated with an increased flux of allochthonous nutrients from the atmosphere or a decrease in light intensity. We did not measure any parameter associated with atmospheric deposition, but a significant increase in the flux of nutrients from the atmosphere would have increased the nutrient concentrations in the upper water column and would inevitably have led to an increase of ρNO_3^- in the NDL, which is typically N-limited in the SCS (Du et al., 2017; Savarino et al., 2007). However, the fact that ρNO_3^- at shallow depths did not change significantly during our 7-day observation period (Figure 3a) was inconsistent with the atmospheric deposition hypothesis. Because of the rainy weather, the PAR at 13:00 was indeed significantly lower on 26 August than on other observation dates (Figure S3). A decrease of light intensity could reduce photoinhibition of *Prochlorococcus* at the surface (Flombaum et al., 2013; Xiao et al., 2019; Xie et al., 2018). The effect of a decrease of light intensity on *Procholorococcus* would therefore have differed between the surface and subsurface. The fact that the changes of

Procholorococcus abundance were almost the same at the surface and at 25 m and 50 m was therefore inconsistent with the photoinhibition scenario (Figure 2d–f). We therefore concluded that both the warm eddy and the brief period of rainy weather were probably not the main factors that caused the three-layer structure of the phytoplankton community to become apparent.

Conclusions and Implications

This study provided strong evidence that the perturbation caused by internal waves made it apparent that the structure of the phytoplankton community in the euphotic zone of South China Sea was best described by a three-layer structure at steady state because the factors that limited phytoplankton growth differed in the three layers (Figure 4). It has been a common assumption that the DCML is an ecologically important feature of stratified oceans since the seminal paper by Yentsch (1965). Primary production in the DCML accounts for 30–70% of water column production, and this layer also accounts for the largest proportion of new production (Cai et al., 2015; Lee Chen et al., 2008). Production in the NRL is much lower because of severe light limitation (Figure S5), but its contribution to particle export flux can be high if grazing rates are high (Landry et al., 2011a). High grazing rates in the NRL and DCML support high rates of regenerated production in the NDL, which would enhance carbon export through the microbial carbon pump (Jiao et al., 2010). The implication is that the concept of a three-layer euphotic zone will facilitate estimates of marine primary production and enhance understanding of the global carbon cycle.

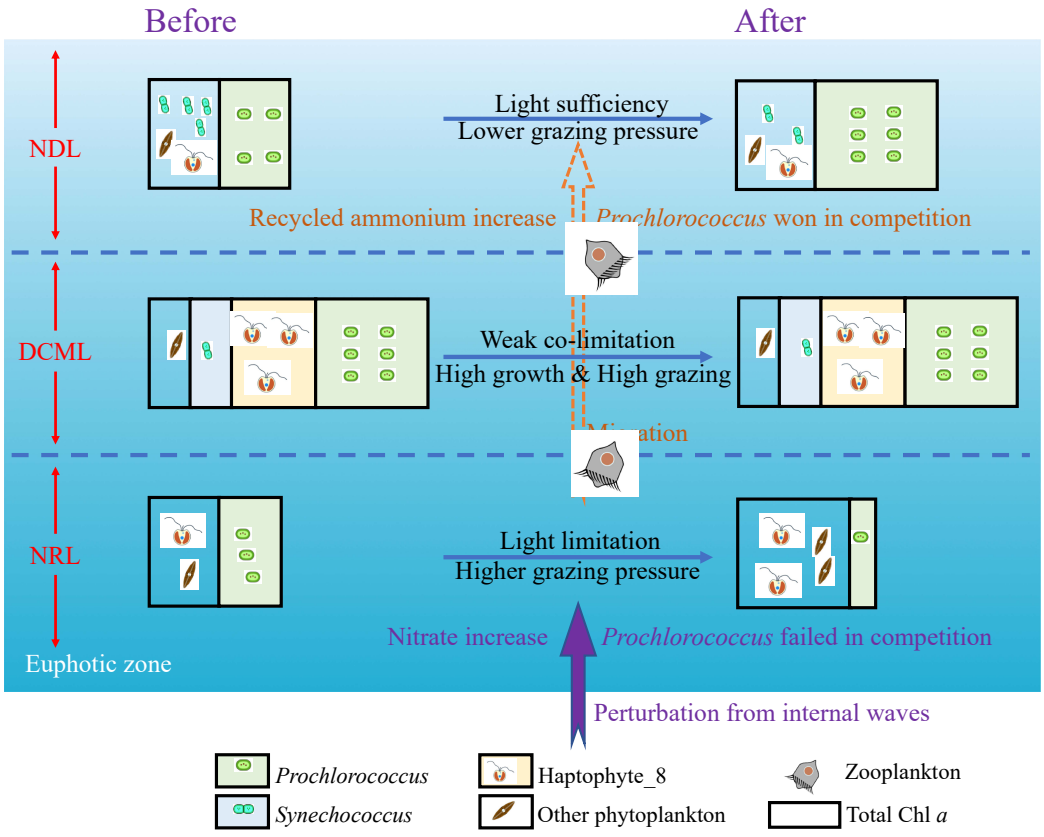

385

386 **Figure 4.** The three-layer structure of the phytoplankton community in the euphotic
387 zone of oligotrophic oceans. In steady state, phytoplankton are restricted by nutrient
388 limitation in the upper nutrient-depleted layer (NDL), by light in the lower
389 nutrient-replete layer (NRL), and by both nutrients and light in the middle deep
390 chlorophyll maximum layer (DCML). When there is a perturbation caused by internal
391 waves, uplifted nitrate stimulates the phytoplankton groups other than
392 *Prochlorococcus* in the NRL, and because of light limitation, phytoplankton biomass
393 is held in check by microzooplankton grazing. The result is a decreased relative
394 abundance of *Prochlorococcus* and unchanged TChl *a*. In the DCML, weak
395 co-limitation by nutrients and light results in high nitrate assimilation rates and high
396 growth rates, but the increased phytoplankton growth rates are balanced by high
397 grazing rates. The result is a stable, high TChl *a* concentration. In the NDL,
398 *Prochlorococcus* benefits from ammonium regenerated by zooplankton that migrate
399 from below. The result is an increased relative abundance of *Prochlorococcus* and
400 increase of TChl *a*.
401

Acknowledgements

This work was funded by the National Natural Science Foundation of China through grants 42206140, 42130401, 91958203, 42141002, 42006019, 42276209, and 42006112, the China Postdoctoral Science Foundation through grant 2021M702728, the Cross-Strait Postdoctoral Fellowship Plan through grant 2021B001, and the Outstanding Postdoctoral Scholarship, State Key Laboratory of Marine Environmental Science at Xiamen University. We thank Dr. Yibin Huang for the gross primary production data and Lizhen Lin for the measurement of pigment samples. We also thank captains and crew of R/V *Shiyan 1* for their cooperation during the field cruises.

Data Availability Statement

Physical-biochemical data collected onboard used in this study can be found in https://data.mendeley.com/datasets/c5rknh37t5.

References

Berube, P. M., et al. (2015), Physiology and evolution of nitrate acquisition in *Prochlorococcus*, *The ISME Journal*, *9*(5), 1195-1207. DOI: 10.1038/ismej.2014.211.

Bouman, H. A., et al. (2006), Oceanographic basis of the global surface distribution of *Prochlorococcus* ecotypes, *Science*, *312*(5775), 918-921. DOI: 10.1126/science.1122692.

Cai, P., D. Zhao, L. Wang, B. Huang, and M. Dai (2015), Role of particle stock and phytoplankton community structure in regulating particulate organic carbon export in a large marginal sea, *Journal of Geophysical Research: Oceans*, *120*(3), 2063-2095. DOI: 10.1002/2014JC010432.

Chen, B., L. Zheng, B. Huang, S. Song, and H. Liu (2013), Seasonal and spatial comparisons of phytoplankton growth and mortality rates due to microzooplankton grazing in the northern South China Sea, *Biogeosciences*, *10*(4), 2775-2785. DOI: 10.5194/bg-10-2775-2013.

Du, C. J., Z. Y. Liu, S. J. Kao, and M. H. Dai (2017), Diapycnal fluxes of nutrients in an oligotrophic oceanic regime: The South China Sea, *Geophysical Research Letters*, *44*(22), 11510-11518. DOI: 10.1002/2017gl074921.

Dugdale, R. C. (1967), Nutrient limitation in the sea: dynamics, identification, and significance, *Limnology and Oceanography*, *12*(4), 685-695. DOI: 10.4319/lo.1967.12.4.0685.

Dugdale, R. C., and F. P. Wilkerson (1986), The use of N-15 to measure nitrogen uptake in eutrophic oceans - experimental considerations, *Limnology and Oceanography*, *31*(4), 673-689. DOI: 10.4319/lo.1986.31.4.0673.

Flombaum, P., et al. (2013), Present and future global distributions of the marine

443 cyanobacteria *Prochlorococcus* and *Synechococcus*, *Proceedings of the National*
444 *Academy of Sciences*, *110*(24), 9824-9829. DOI: 10.1073/pnas.1307701110.
445 Fonda Umani, S., V. Tirelli, A. Beran, and B. Guardiani (2005), Relationships
446 between microzooplankton and mesozooplankton: competition versus predation
447 on natural assemblages of the Gulf of Trieste (northern Adriatic Sea), *Journal of*
448 *Plankton Research*, *27*(10), 973-986. DOI: 10.1093/plankt/fbi069.
449 Forget, G., J. M. Campin, P. Heimbach, C. N. Hill, R. M. Ponte, and C. Wunsch
450 (2015), ECCO version 4: an integrated framework for non-linear inverse
451 modeling and global ocean state estimation, *Geoscientific Model Development*
452 *Discussions*, *8*(10), 3071-3104. DOI: 10.5194/gmd-8-3071-2015.
453 Furuya, K., M. Hayashi, Y. Yabushita, and A. Ishikawa (2003), Phytoplankton
454 dynamics in the East China Sea in spring and summer as revealed by
455 HPLC-derived pigment signatures, *Deep Sea Research Part II: Topical Studies*
456 *in Oceanography*, *50*(2), 367-387. DOI: 10.1016/S0967-0645(02)00460-5.
457 Garrett, C. (2003), Internal tides and ocean mixing, *Science*, *301*(5641), 1858-1859.
458 DOI: 10.1126/science.1090002.
459 Garwood, J. C., R. C. Musgrave, and A. J. Lucas (2020), Life in internal waves,
460 *Oceanography*, *33*(3), 38-49. DOI: 10.5670/oceanog.2020.313.
461 Guo, C., H. Liu, L. Zheng, S. Song, B. Chen, and B. Huang (2014), Seasonal and
462 spatial patterns of picophytoplankton growth, grazing and distribution in the East
463 China Sea, *Biogeosciences*, *11*(7), 1847-1862. DOI: 10.5194/bg-11-1847-2014.
464 Hays, G. C. (2003), A review of the adaptive significance and ecosystem
465 consequences of zooplankton diel vertical migrations, *Migrations and Dispersal*
466 *of Marine Organisms*, *503*(1-3), 163-170. DOI:
467 10.1023/B:HYDR.0000008476.23617.b0.

468 Huang, B., J. Hu, H. Xu, Z. Cao, and D. Wang (2010), Phytoplankton community at
469 warm eddies in the northern South China Sea in winter 2003/2004, *Deep Sea*
470 *Research Part II: Topical Studies in Oceanography*, *57*(19), 1792-1798. DOI:
471 10.1016/j.dsr2.2010.04.005.
472 Jiao, N., et al. (2010), Microbial production of recalcitrant dissolved organic matter:
473 long-term carbon storage in the global ocean, *Nature Reviews Microbiology*, *8*(8),
474 593-599. DOI: 10.1038/nrmicro2386.
475 King, F. D., T. L. Cucci, and D. W. Townsend (1987), Microzooplankton and
476 macrozooplankton glutamate dehydrogenase as indices of the relative
477 contribution of these fractions to ammonium regeneration in the Gulf of Maine,
478 *Journal of Plankton Research*, *9*(2), 277-289. DOI: 10.1093/plankt/9.2.277.
479 Landry, M. R., and R. P. Hassett (1982), Estimating the grazing impact of marine
480 micro-zooplankton, *Marine Biology*, *67*(3), 283-288. DOI:
481 10.1007/BF00397668.
482 Landry, M. R., K. E. Selph, and E. J. Yang (2011a), Decoupled phytoplankton growth
483 and microzooplankton grazing in the deep euphotic zone of the eastern equatorial
484 Pacific, *Marine Ecology Progress Series*, *421*, 13-24. DOI: 10.3354/meps08792.
485 Landry, M. R., M. Decima, M. P. Simmons, C. C. S. Hannides, and E. Daniels (2008),
486 Mesozooplankton biomass and grazing responses to cyclone opal, a subtropical
487 mesoscale eddy, *Deep Sea Research Part II: Topical Studies in Oceanography*,
488 *55*(10), 1378-1388. DOI: 10.1016/j.dsr2.2008.01.005.
489 Landry, M. R., K. E. Selph, A. G. Taylor, M. Décima, W. M. Balch, and R. R.
490 Bidigare (2011b), Phytoplankton growth, grazing and production balances in the
491 HNLC equatorial Pacific, *Deep Sea Research Part II: Topical Studies in*
492 *Oceanography*, *58*(3), 524-535. DOI: 10.1016/j.dsr2.2010.08.011.

493 Lee Chen, Y.-l., H.-Y. Chen, S.-h. Tuo, and K. Ohki (2008), Seasonal dynamics of
494 new production from *Trichodesmium* N_2 fixation and nitrate uptake in the
495 upstream Kuroshio and South China Sea basin, *Limnology and Oceanography*,
496 *53*(5), 1705-1721. DOI: 10.4319/lo.2008.53.5.1705.
497 Lin, H., Z. Liu, J. Hu, D. Menemenlis, and Y. Huang (2020), Characterizing meso- to
498 submesoscale features in the South China Sea, *Progress in Oceanography*, *188*,
499 102420. DOI: 10.1016/j.pocean.2020.102420.
500 Lucas, A. J., C. L. Dupont, V. Tai, J. L. Largier, B. Palenik, and P. J. S. Franks (2011),
501 The green ribbon: Multiscale physical control of phytoplankton productivity and
502 community structure over a narrow continental shelf, *Limnology and*
503 *Oceanography*, *56*(2), 611-626. DOI: 10.4319/lo.2011.56.2.0611.
504 Ma, L., W. Xiao, E. A. Laws, X. Bai, K.-P. Chiang, X. Liu, J. Chen, and B. Huang
505 (2020), Responses of phytoplankton communities to the effect of internal
506 wave-powered upwelling, *Limnology and Oceanography*, *66*(4), 1083-1098.
507 DOI: 10.1002/lno.11666.
508 Mackey, M. D., D. J. Mackey, H. W. Higgins, and S. W. Wright (1996), CHEMTAX -
509 a program for estimating class abundances from chemical markers: application to
510 HPLC measurements of phytoplankton, *Marine Ecology Progress Series*, *144*(1),
511 265-283. DOI: 10.3354/meps144265.
512 Moore, L. R., A. F. Post, G. Rocap, and S. W. Chisholm (2002), Utilization of
513 different nitrogen sources by the marine cyanobacteria *Prochlorococcus* and
514 *Synechococcus*, *Limnology and Oceanography*, *47*(4), 989-996. DOI:
515 10.4319/lo.2002.47.4.0989.
516 Omand, M. M., J. J. Leichter, P. J. S. Franks, R. T. Guza, A. J. Lucas, and F.
517 Feddersen (2011), Physical and biological processes underlying the sudden

surface appearance of a red tide in the nearshore, *Limnology and Oceanography*, *56*(3), 787-801. DOI: 10.4319/lo.2011.56.3.0787.

Savarino, J., J. Kaiser, S. Morin, D. M. Sigman, and M. H. Thiemens (2007), Nitrogen and oxygen isotopic constraints on the origin of atmospheric nitrate in coastal Antarctica, *Atmospheric Chemistry and Physics*, *7*(8), 1925-1945. DOI: 10.5194/acp-7-1925-2007.

Sharples, J., C. M. Moore, A. E. Hickman, P. M. Holligan, J. F. Tweddle, M. R. Palmer, and J. H. Simpson (2009), Internal tidal mixing as a control on continental margin ecosystems, *Geophysical Research Letters*, *36*(23), L23603. DOI: 10.1029/2009gl040683.

Sharples, J., et al. (2007), Spring-neap modulation of internal tide mixing and vertical nitrate fluxes at a shelf edge in summer, *Limnology and Oceanography*, *52*(5), 1735-1747. DOI: 10.4319/lo.2007.52.5.1735.

Torres, H. S., P. Klein, D. Menemenlis, B. Qiu, Z. Su, J. Wang, S. Chen, and L.-L. Fu (2018), Partitioning ocean motions into balanced motions and internal gravity waves: a modeling study in anticipation of future space missions, *Journal of Geophysical Research: Oceans*, *123*(11), 8084-8105. DOI: 10.1029/2018JC014438.

Tuerena, R. E., R. G. Williams, C. Mahaffey, C. Vic, J. A. M. Green, A. Naveira‐Garabato, A. Forryan, and J. Sharples (2019), Internal tides drive nutrient fluxes into the deep chlorophyll maximum over mid-ocean ridges, *Global Biogeochemical Cycles*, *33*(8), 995-1009. DOI: 10.1029/2019gb006214.

Villamaña, M., et al. (2017), Role of internal waves on mixing, nutrient supply and phytoplankton community structure during spring and neap tides in the upwelling ecosystem of Ría de Vigo (NW Iberian Peninsula), *Limnology and*

Oceanography, *62*(3), 1014-1030. DOI: 10.1002/lno.10482.

Wang, L., B. Huang, E. A. Laws, K. Zhou, X. Liu, Y. Xie, and M. Dai (2018), Anticyclonic eddy edge effects on phytoplankton communities and particle export in the northern South China Sea, *Journal of Geophysical Research: Oceans*, *123*(11), 7632-7650. DOI: 10.1029/2017JC013623.

Wang, Y.-H., C.-F. Dai, and Y.-Y. Chen (2007), Physical and ecological processes of internal waves on an isolated reef ecosystem in the South China Sea, *Geophysical Research Letters*, *34*(18), L18609. DOI: 10.1029/2007gl030658.

Webb, K. L., and R. E. Johannes (1967), Studis of the release of dissolved free amino acids by marine zooplankton, *Limnology and Oceanography*, *12*(3), 376-382. DOI: 10.4319/lo.1967.12.3.0376.

Whalen, C. B., C. de Lavergne, A. C. Naveira Garabato, J. M. Klymak, J. A. MacKinnon, and K. L. Sheen (2020), Internal wave-driven mixing: governing processes and consequences for climate, *Nature Reviews Earth & Environment*, *1*(11), 606-621. DOI: 10.1038/s43017-020-0097-z.

Wong, G. T. F., T.-L. Ku, M. Mulholland, C.-M. Tseng, and D.-P. Wang (2007), The SouthEast Asian Time-series Study (SEATS) and the biogeochemistry of the South China Sea—an overview, *Deep Sea Research Part II: Topical Studies in Oceanography*, *54*(14), 1434-1447. DOI: 10.1016/j.dsr2.2007.05.012.

Xiao, W., X. Liu, A. J. Irwin, E. A. Laws, L. Wang, B. Chen, Y. Zeng, and B. Huang (2018), Warming and eutrophication combine to restructure diatoms and dinoflagellates, *Water Research*, *128*, 206-216. DOI: 10.1016/j.watres.2017.10.051.

Xiao, W., E. A. Laws, Y. Xie, L. Wang, X. Liu, J. Chen, B. Chen, and B. Huang (2019), Responses of marine phytoplankton communities to environmental

568 changes: New insights from a niche classification scheme, *Water Research*, *166*,
569 115070. DOI: 10.1016/j.watres.2019.115070.
570 Xie, Y., E. A. Laws, L. Yang, and B. Huang (2018), Diel patterns of variable
571 fluorescence and carbon fixation of picocyanobacteria
572 *Prochlorococcus*-dominated phytoplankton in the South China Sea basin,
573 *Frontiers in Microbiology*, *9*. DOI: 10.3389/fmicb.2018.01589.
574 Yentsch, C. S. (1965), Distribution of chlorophyll and phaeophytin in the open ocean,
575 *Deep Sea Research and Oceanographic Abstracts*, *12*(5), 653-666. DOI:
576 10.1016/0011-7471(65)91864-4.
577 Zhao, Z. (2014), Internal tide radiation from the Luzon Strait, *Journal of Geophysical*
578 *Research: Oceans*, *119*(8), 5434-5448. DOI: 10.1002/2014JC010014.
579 Zhao, Z. (2020), Southward internal tides in the northeastern South China Sea,
580 *Journal of Geophysical Research: Oceans*, *125*(11), e2020JC016554. DOI:
581 10.1029/2020jc016554.
582